

Sand migration simulation during gas production from gas hydrate reservoir at Kuparuk 7-11-12 site in the Prodhoe Bay Unit, Alaska

Shun Uchida,^{*,†} Yongkoo Seol,[‡] and Koji Yamamoto[¶]

[†]*Rensselaer Polytechnic Institute, Troy, New York 12180, United States*

[‡]*National Energy Technology Laboratory - U.S. Department of Energy, Morgantown, West
Virginia 26505, United States*

[¶]*Japan Oil, Gas and Metals National Corporation, Chiba 261-0025, Japan*

E-mail: uchids@rpi.edu

Abstract

Uncontrolled sand production impedes continuous gas production from hydrate reservoir as observed in the past field-scale gas production tests. Sand mobilization is strongly linked with sediment deformation and high pressure gradient. Sand production is when the mobilized sands reach the well. Throughout gas production from hydrate reservoir, because of hydrate dissociation, deformation and pressure gradient change both in time and space. Therefore, it is necessary to consider the entire processes to identify where sands are likely mobilized and how much mobilized sands could reach the well. This study utilizes a coupled thermal, hydrological, chemical and mechanical (thermo-hydro-chemo-mechanical) sand migration model to simulate a-year-long gas production from hydrate reservoir at Kuparuk 7-11-12 site in the Prodhoe Bay Unit, Alaska. It is found that sands would mainly come from the lower portion of the production zone where faster hydrate dissociation occurs. The relatively

faster hydrate dissociation coupled with the fact that hydrate-bearing sediments and hydrate-free sediments have similar stiffness but different strengths causes complex stress transfer, which results in excessive shear deformation when the upper portion of the production zone starts to dissociate. This is evident not only near the well but also away from the well, leading to a large amount of sand mobilization. Another focus of the modeling study is evaluation of the effect of sand migration on gas production. Comparison of two extreme cases with sandscreen and without sandscreen - suggests that migrated and settled solids around sand control device can prevent pressure drop across the near-wellbore zone and lead to reduction of gas production rate.

Introduction

A long-term continuous gas production from hydrate reservoir still remains a challenge. One of the obstacles need to be overcome is uncontrolled sand production, a problem which mobilized sands reach to the well far excessively than in manageable manner, resulting in severe damage of operational equipments and well clogging. As observed in the past, about half of the field-scale gas production tests from hydrate reservoir encountered uncontrolled sand production, leading to early abandonment of the production wells^{1,2}. Even with the presence of sand screen, sand flow was observed inside the well, which led to early termination of the operation³. This could imply that accumulation of sand behind the screen might have caused severe sediment deformation around the well. In specific, in the case of the offshore production test conducted in the Eastern Nankai Trough area, sand control devices was set for excluding sand inflow into the borehole. However, recent analysis of production and monitoring data indicated development of “skin” across the near-wellbore zone possibly caused by low apparent permeability zone due to potentially clogging of the sand control device and formation around the well^{4,5}. International collaboration between U.S. and Japan plans gas production from gas hydrate reservoir in the Prudhoe Bay Unit, Alaska North Slope. Therefore, it is important to model sand migration during the planned test and

predict where sands might come from and understand the effect of sand accumulation near the well on the mechanical behavior of sediments over a period of one year.

The production site, Kuparuk 7-11-12, in the Prodhoe Bay Unit, Alaska, has been identified an ideal site for gas hydrate production with the past extensive scientific research and it is confirmed that the site contains two high quality gas hydrate reservoirs^{6,7}. Furthermore, through logging data and side-wall coring, the detailed characterization of reservoir and non-reservoir units of the site has been established^{8,9}. Based on these findings, this study simulates sand migration during the planned gas production at the 7-11-12 site. The analysis is carried out using the coupled thermal, hydrological, chemical and mechanical (thermo-hydro-chemo-mechanical) sand migration model that is originally developed by Uchida et al.¹⁰. To evaluate the effect of development of “skin”, two extreme cases are set to simulate conditions of sand inflow: non-sand control case in which produced solid can flow into the well freely; and perfect sand exclusion case in which the entire migrated sand with gas and water should stop and settle down in the domain near the surface of the well. The former case is not applicable in unconsolidated or weakly consolidated gas hydrate-bearing sediments, and the latter case is not realistic because practical sand control devices such as sandscreen are designed to allow inflow of some fine sediments to prevent total clogging of the sand control device. Nonetheless, those two extreme cases may provide insight into the mechanism of sand production and effects of geomechanical conditions on the occurrence of sand motion (the former case), and potential adverse effects of sand control devices (the latter case).

The following sections describe brief summary of sand migration model, the geometry and initial condition of the site and the results of sand migration analyses.

Modified thermo-hydro-mechanical sand migration model

Uchida et al.¹⁰ developed sand migration model for hydrate reservoir that incorporates the

mobilization of sands, sand flow and its coupling effect with pressure, temperature and the sediment responses into thermo-hydro-chemo-mechanical formulation that solves governing equations for soil, water, gas and hydrate. The model was used for history matching including sand production during the past 2013 Nankai offshore gas production test and for understanding of sand mobilization and migration phenomena in interbedded sediments^{11,12}. Furthermore, the authors previously studied the variance-based sensitivity of the model parameters and determined the most influential parameters that govern sand migration processes¹³. This has resulted in eliminating three model parameters (out of six) that incorporated sand settling, sand lifting, sand flowing with gas, and effective stress reduction by sand mobilization. The simplified formulation is as follows. The model considers two statuses for sand, stationary and flowing:

$$V_s = V_{ss} + V_{fs} \quad (1)$$

where V_s is the sand volume, V_{ss} is the stationary sand volume and V_{fs} is the flowing sand volume. The stationary sand will be mobilized (i.e. $dV_{ss} < 0$) when there is a mobilization potential and also when the hydraulic gradient is larger than the critical value:

$$\begin{aligned} dV_{ss} &= 0 & \text{when } |\mathbf{i}_w| < i_c(1 - S_h)^{-\omega_3} \\ dV_{ss} &= -V_{ss}M_p dt & \text{when } |\mathbf{i}_w| \geq i_c(1 - S_h)^{-\omega_3} \end{aligned} \quad (2)$$

where \mathbf{i}_w is the hydraulic gradient vector, i_c is the critical hydraulic gradient when fully water saturated below which no sand mobilization occurs, S_h is the hydrate saturation, ω_3 is the model parameter that determines the effect of hydrate on the critical gradient and M_p is the mobilization potential which is incrementally given by:

$$dM_p = \omega_4 d\epsilon_d + \frac{dV_{ss}}{V_{ss}} \quad (3)$$

where ϵ_d is the deviatoric strain and ω_4 is the model parameter that converts the strain into

the potential. Eq. (3) states that mobilization potential increases with deviatoric (shear) deformation but reduces with the actual mobilization, which could lead to $M_p \rightarrow 0$ (depletion of the potential) if no deviatoric deformation develops.

The volume of flowing sand increases with the mobilization and sand flow:

$$dV_{fs} = -dV_{ss} - \nabla \cdot \mathbf{q}_{fs} V dt \quad (4)$$

where V is the control volume, $\nabla \cdot \mathbf{q}_{fs}$ is the divergence of sand flow flux \mathbf{q}_{fs} , V is the control volume and t is time. Combining Eq. (2) & Eq. (4), the incremental form of sand volume is given by:

$$dV_s = -\nabla \cdot \mathbf{q}_{fs} V dt \quad (5)$$

This affects the void volume ($= V - V_s$), so that it changes pressure and saturations, leading to change in the fluid compressibility, permeability and heat capacity. The sand flow also changes the temperature because of the heat that brings into the domain. Therefore, sand migration is fully coupled with thermo-hydro-chemo-mechanical processes involved throughout gas production from hydrate reservoir. The details of the model such as Darcy's based sand flow model, can be found in the original work¹⁰. Values of the three parameters adopted in this study are listed in Table 1. These values are similar to those used for the 2013 Nankai test simulation¹¹, in which the parameter values were determined to match the reported produced sand volume ($\approx 25 \text{ m}^3$). However, the adopted values in this study are somewhat arbitrary and it is likely that these values would be different when post-production history matching or experimental studies focusing on the conditions at Kuparuk 7-11-12 site are conducted. In general, greater i_c and ω_3 reduces sand migration while greater ω_4 increases sand migration. This study focuses on sand migration and fines migration is not considered. In order to prevent clays from being mobilized, the mobilization potential is kept zero by setting $\omega_4 = 0$ for the clay layers.

Table 1: Sand migration model parameters

	value	Eq#
critical hydraulic gradient i_c	5.0	(2)
power for hydrate effect ω_3	10.0	(2)
shear to mobilization potential ω_4	1.0	(3)

Model of the Kuparuk 7-11-12 site

Geometry and initial conditions

An idealized model, which is shown in Fig 1, representing the Kuparuk 7-11-12 site is constructed based on the geological findings by Collett et al.⁷, Tamaki et al.¹⁴. This study focuses lower reservoir, Unit B, of the two high-quality hydrate reservoirs found at the Kuparuk 7-11-12. The model domain is axisymmetric and the top boundary corresponds to the depth of $z = 830$ m below sea level (bsl), the bottom boundary is at $z = 880$ m bsl and the far-field boundary is at $r = 150$ m. The domain is discretized vertically into 40 elements with the finest element thickness being approximately 0.7 m around the production zone while radially into 40 elements with the finest width being approximately 0.8 m around the well. Because of computational efficiency, this model is smaller and coarser than the model used for gas production simulation at the Kuparuk 7-11-12 site by Myshakin et al.⁹. The top, bottom and far-field boundaries have the constant pressure, temperature and effective stresses. The pore pressure is hydrostatic and thermal gradient is 0.037 K/m. At the well boundary, the sediments are allowed to move only in the vertical direction. The well boundary is insulated and impermeable except the production zone, which is located between 847 m and 857 m bsl.

For the initial properties, this study follows the work by Myshakin et al.⁹ based on the hydrate saturation and permeability profile determined by Tamaki et al.¹⁴. In their work⁹, there are three cases for the hydrate saturation, intrinsic and effective permeability variations and this study corresponds to their Case C. This is because Case C is deemed to induce

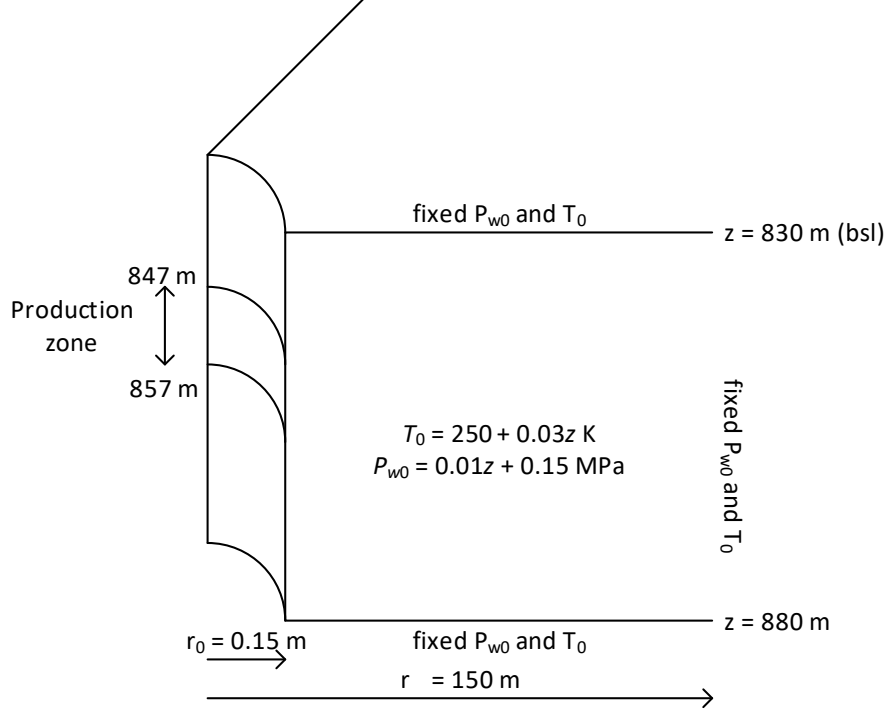


Figure 1: Geometry and boundary conditions for the Kupruk model

greatest hydrate dissociation, which causes sand migration due to development of sediment deformation and hydraulic gradient. Fig. 2 presents (a) hydrate saturation, (b) intrinsic permeability $\sqrt{K_r K_z}$ and effective permeability $\sqrt{K_{hr} K_{hz}}$, (c) the permeability anisotropic ratio K_{hr}/K_{hz} , and (d) porosity n . The layer with the intrinsic permeability $\sqrt{K_r K_z} < 1$ mD (milli Darcy) is classified as a clay layer. The soil lithology is also included in Fig. 2. While the saturation and permeability profile by Myshakin et al.⁹ has an approximately 0.15 m resolution, the model adopted in this study is larger thickness (≈ 0.7 m). In order to accurately capture the total hydrate volume and the permeability heterogeneity, the vertically heterogeneous hydrate saturation is averaged through:

$$S_h = \frac{\sum_i S_{h,i} \Delta z_i}{\sum_i \Delta z_i} \quad (6)$$

where $S_{h,i}$ is the estimated hydrate saturation from the data, Δz_i is the interval of each data point and $\sum_i \Delta z_i$ is the height of the model element and i is the number of data points within

the element. For the permeability, it is important to consider the flow direction as opposed to a simple averaging method as Eq. (6). The radial flow is parallel to the sediment layering and the vertical flow is perpendicular to the sediment layering. This results in:

$$K_r = \frac{\sum_i K_i \Delta z_i}{\sum_i \Delta z_i} \quad (7)$$

$$\frac{\sum_i \Delta z_i}{K_z} = \sum_i \frac{\Delta z_i}{K_i} \quad (8)$$

where K_i is the estimated intrinsic permeability from the data, K_r is the radial intrinsic permeability for the model element and K_z is the vertical intrinsic permeability for the model element. Similarly, for the effective permeability:

$$K_{hr} = \frac{\sum_i K_{h,i} \Delta z_i}{\sum_i \Delta z_i} \quad (9)$$

$$\frac{\sum_i \Delta z_i}{K_{hz}} = \sum_i \frac{\Delta z_i}{K_{h,i}} \quad (10)$$

where $K_{h,i}$ is the estimated effective permeability from the data, K_{hr} is the radial effective permeability for the model element and K_{hz} is the vertical effective permeability for the model element. The simple power law to relate the effective permeability by Masuda et al.¹⁵ is adopted and thus the intrinsic permeability can be rewritten as:

$$K_{hr} = K_r (1 - S_h)^{N_r} \quad (11)$$

$$K_{hz} = K_z (1 - S_h)^{N_z} \quad (12)$$

where N_r and N_z is the power for the radial and vertical direction, respectively, which are estimated based on K_{hr} , K_r and S_h for N_r while K_{hz} , K_z and S_h for N_z . From Eqs. (11)–(12), the permeability anisotropic ratio is given by:

$$\frac{K_{hr}}{K_{hz}} = \frac{K_r}{K_z} (1 - S_h)^{N_r - N_z} \quad (13)$$

Eq. (13) clearly shows the anisotropic ratio changes with hydrate saturation and it is different from the value associated with the intrinsic permeability. When hydrate is completely dissociated, the anisotropic ratio of effective permeability becomes that of intrinsic permeability, $K_{hr}/K_{hz} = K_r/K_z$ when $S_h = 0$. It is important to state that the anisotropic ratio is established to facilitate the heterogeneity existing within the model elements and also resulting difference in parallel and perpendicular flow to layering. When the thickness of the model is equal to the measurement interval, that is, $\sum_i \Delta z_i = \Delta z_i$ ($i = 1$), or when the properties are homogeneous within i layers, it leads to isotropic condition, that is, $K_r = K_z$ and $N_r = N_z$.

Furthermore, in this study the intrinsic permeability changes according to void volume change caused by sediment deformation as well as solid volume change caused by sand migration. It follows the Kozeny-Carman equation^{16,17}, which is given by:

$$K_{r,z} \propto \frac{V_v^3}{V_s^2} \quad (14)$$

where $K_{r,z}$ is both radial and vertical permeability and V_v is the void volume.

Gas production will be initiated by stepping-depressurization including two shut-in periods. Fig. 3 shows the applied depressurization in this study and this corresponds to Scenario 4 in Myshakin et al.⁹. There are two shut-in periods between 85-100 days and 215-220 days, corresponding potential events such as maintenance that requires production shut-downs. The shut-in period is likely to cause drastic hydraulic gradient change, especially when re-depressurization is applied. Therefore it is more likely to induce sand migration.

Hydrate-bearing soil behavior

The behavior of hydrate-bearing sediments is modeled using the methane hydrate critical state model.¹⁸ The soil samples are recovered from the site using side-wall coring technology and analyzed by Collett et al.⁷, Yoneda et al.⁸. Fig. 4 shows the triaxial test data of the

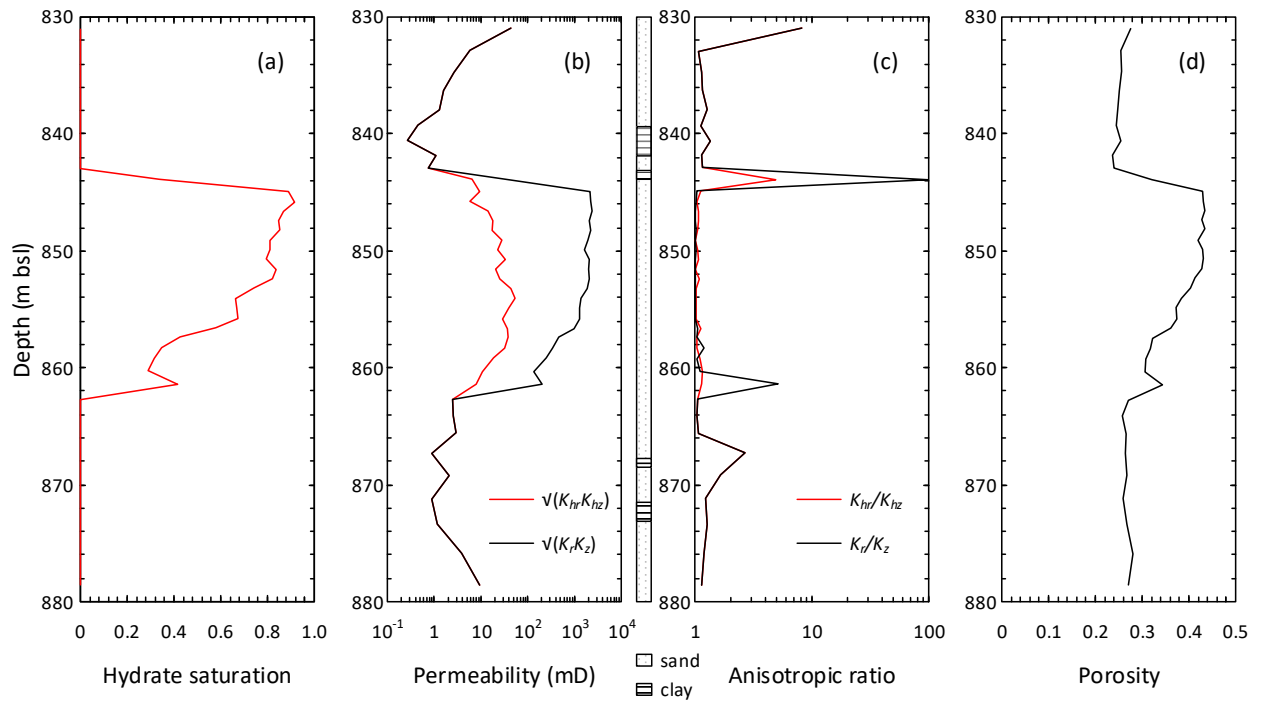


Figure 2: The initial conditions of (a) hydrate saturation, (b) intrinsic and effective permeability, (c) anisotropic ratio and (d) porosity

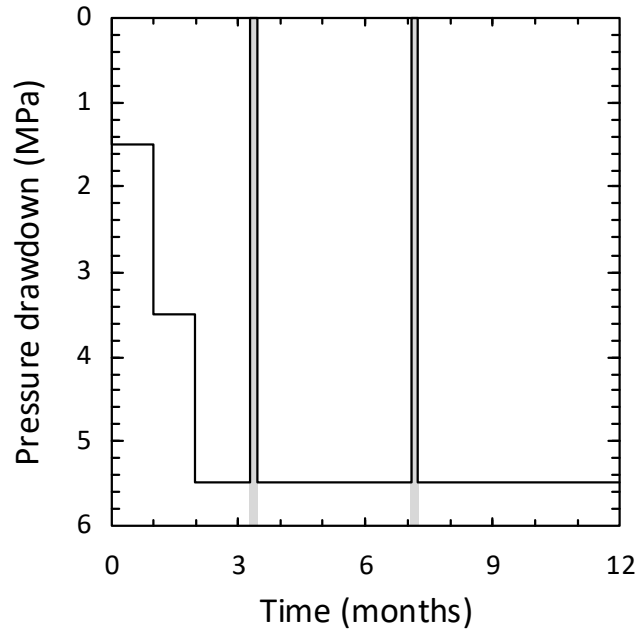


Figure 3: Applied pressure drawdown over a one-year period

soil from the site and the model fitting using the methane hydrate critical state model¹⁸. The determined model parameters are presented in Table 2. One key observation is that there is a relatively large difference between the peak strength of the recovered hydrate-bearing sediments and the strength of the hydrate-free sediments at the same strain level, approximately $\epsilon_a = 2\%$ as can be seen in Fig. 4a. On the other hand, the stiffness (slope of $q - \epsilon_a$ curve) as well the volumetric strain at $\epsilon_a \approx 2\%$ are almost the same. This means the stress will almost be equally distributed between hydrate-bearing and hydrate-free sediments but once hydrate dissociates the stress carried by the hydrate-bearing sediments will be transferred to hydrate-free sediments. This could make the hydrate-free sediments carrying more stresses than dissociating hydrate-bearing sediments.

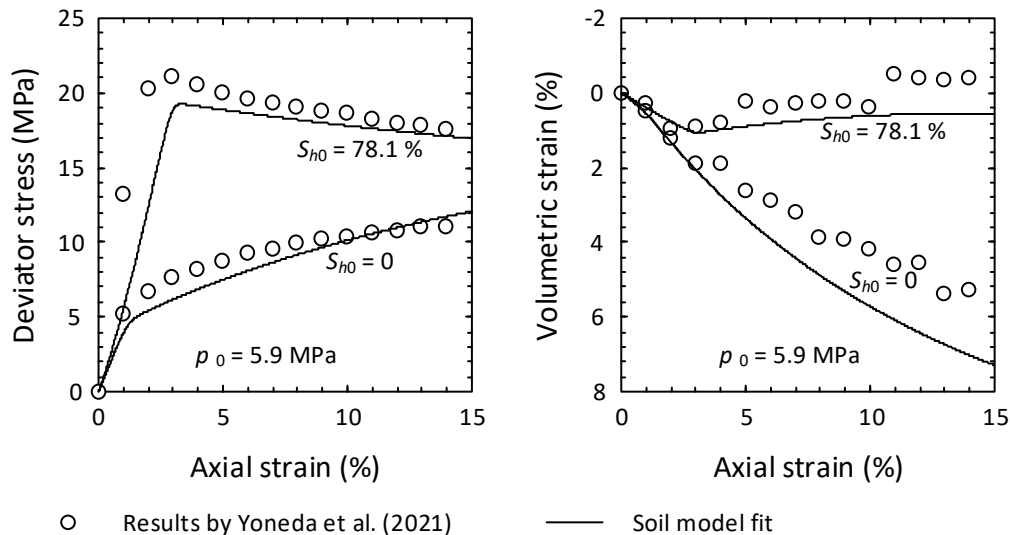


Figure 4: Drained triaxial tests on the soil from the Kuparuk 7-11-12 site

Results and discussion

This study considers cases with and without sandscreen, the latter of which is presented first. Figs. 5a & b present the changes in (a) pore pressure and (b) hydrate saturation at $t = 4, 8$ and 12 months. The depressurization is effective and since the well pressure is almost constant, the pore pressure gradient slightly decreases with time due to increase in

Table 2: Methane hydrate critical state model parameters

parameters	value
critical state stress ratio M	1.46
slope of norm. comp. line λ	0.19
slope of swelling line κ	0.026
Poisson's ratio ν	0.31
initial preconsolidation stress p'_{cs0}	8.6 MPa
pre-yield plasticity u	500
Hydrate strength contribution	$18.1 (S_h \exp(-15\epsilon_d^p))^{0.1}$ MPa
Hydrate stiffness contribution	$90S_h \exp(-15\epsilon_d^p)$ MPa

the permeability caused by hydrate dissociation. Hydrate dissociation continues and evolves throughout and hydrate dissociation is faster in the lower portion of gas hydrate zone. This is because the intrinsic permeability of the lower portion of the sediments is greater, bringing more heat from the far-field.

Fig. 5c presents the changes in the stress ratio at the aforementioned times, together with deformation represented with the black vectors. The vectors are scaled by the 50 cm vector in the legend and point the direction of deformation. The sediments mainly deforms towards the lower part of the production zone, where significant hydrate dissociation is observed. In order to understand mode of deformation, the evolution of stress ratio q/p' is investigated where q is the deviatoric stress that causes distortion while p' is the mean effective stress that causes volume change. The initial value of the stress ratio is $q/p' = 0.75$. Since depressurization causes increase in p' , it is common to see the reduction in q/p' during gas hydrate production, especially in a short term (days), as previously reported¹¹. This implies that the deformation is more in volumetric mode. This is evident where the hydrate is currently dissociating, for example, upper part of the hydrate zone near the well at $t = 4$ months, which is moving away from the well with time. However, the significant increase in q/p' is also evident, especially in the lower portion of the hydrate zone. This indicates that deformation is more in deviatoric mode that changes shape. The area corresponds to where hydrate is almost entirely dissociated. This implies that, due to hydrate dissociation leading

to stress redistribution, the hydrate-bearing sediments are distorted. This is also attributed to the fact that the stiffness of the hydrate-bearing and hydrate-free sediments is almost same while the strength reduction is significant at these strain level. As a result, stress relaxation happening with dissociating hydrate-bearing sediments causes the hydrate-free sediments deform more easily.

Fig. 6 presents the change in the sand volume in a control volume $\Delta V_s/V$ over time. The negative value denotes reduction in sand volume. As can be seen, sands are mobilized, migrated towards the well and thus removed especially where the intensive deviatoric deformation is observed. This is because the sand production potential, presented in Eq. (3), increases with deviatoric strain. It is normally near the well that shows a significant deviatoric deformation because of wellbore expansion. In a long-term gas production, the deviatoric deformation extends further away from the well and consequently sands are migrating from far away from the well. The increase in $\Delta V_s/V$ means the increase in the sand volume, implying the migration of sands into the area where only small amount of sands is mobilized.

It is also interesting to note that the sand volume increases with time in the lower part of the reservoir. This is because sand is heavier than water so that migrating sands will fall if the radial flow is not dominant. Since the amount of mobilized sands increases with time, the accumulation of sands in the region where the flowrate is small becomes noticeable with time.

Sand control devices might cause adverse effects if the entire migrating sands are blocked at the sandscreen because they should clog the pore throat of the screen and sediments near-by. In order to investigate the effect of sandscreen on reservoir response, this study also considers the simulation with sandscreen. In this model, the sandscren is constructed by simply blocking all the sand flow at the well boundary, accumulating all the migrating sands at the first zone adjacent to the well. In addition, the flowing sands are assumed to continue to move freely towards well and the sediments themselves do not block the flowing sands,

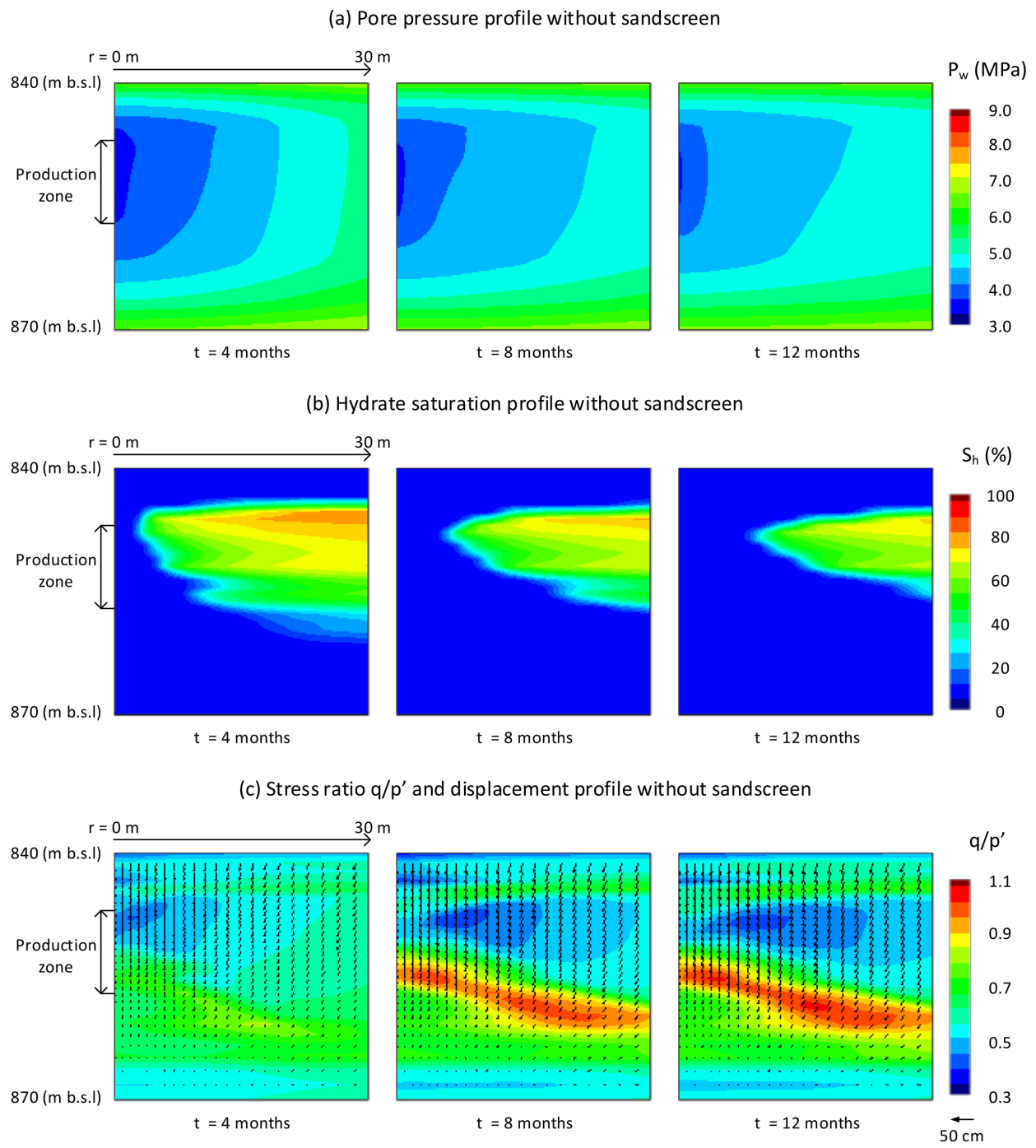


Figure 5: Reservoir responses (a) pore pressure, (b) hydrate saturation and (c) stress ratio without the sandscreen model

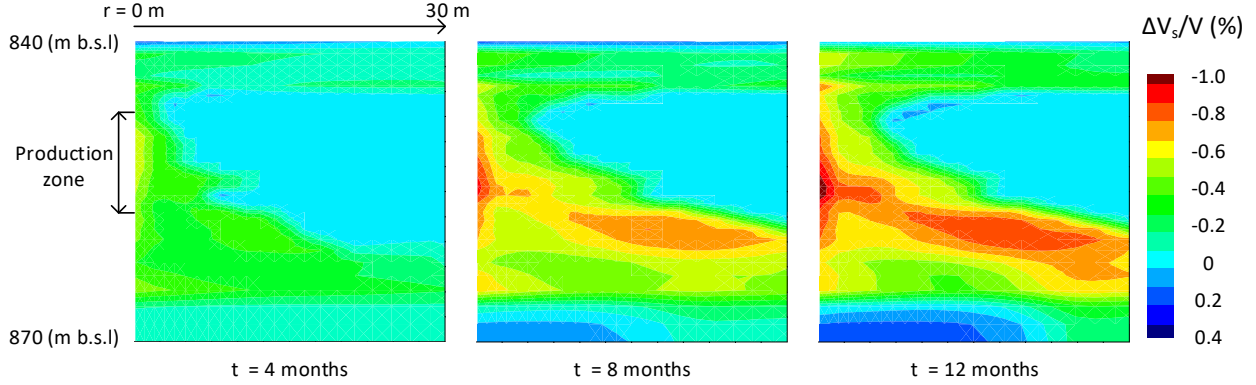


Figure 6: Change in sand volume without the sandscreen model

even though in reality there should be limit for the size of sands passing through pores. Accumulated sands at the well are assumed to reside in the pores of the soil adjacent to the well, reducing the pore volume, and this could eventually lead to zero porosity condition. For actual soil behavior, there would a limit for packing density and therefore zero porosity condition will not happen. However, this study does not consider the effects of particle size or particle size distribution on sand migration through pores and thus zero porosity condition could occur. Although this is highly unlikely, this study assumes it as an extreme condition. Furthermore, in reality, small-sized particles would flow through a sandscreen according to its design, while this model blocks them entirely. Again, the results of this study therefore would be treated as an extreme scenario.

Fig. 7 presents (a) pore pressure change and (b) hydrate saturation change when sandscreen is modeled. Depressurization is significantly hindered and, as a result, hydrate dissociation hardly occurs. This is because the migrating sands are modeled to remain in the first adjacent zone to the well, quickly filling the pores and eventually the intrinsic permeability reduces to almost zero because of the Kozney-Carman equation,^{16,17} presented in Eq. (14). It will be revealed later that the complete closure occurs at around 2 months into the operation. The pore pressure around the production well at 2 months is approximately 3 MPa but at 4 months it is already recovered to about 5 MPa as shown in Fig. 7a. A slight hydrate dissociation is evident at 4 months near the production zone but the hydrate saturation

increases over time, indicating that hydrate reformation occurs due to pressure recovery as shown in Fig. 7b. Fig. 8 shows the change in the sand volume in a control volume over time. The initial value of $1 - V_s/V$ is equal to porosity and thus $\Delta V_s/V \approx 40\%$ indicates a full closure of the sediment pores.

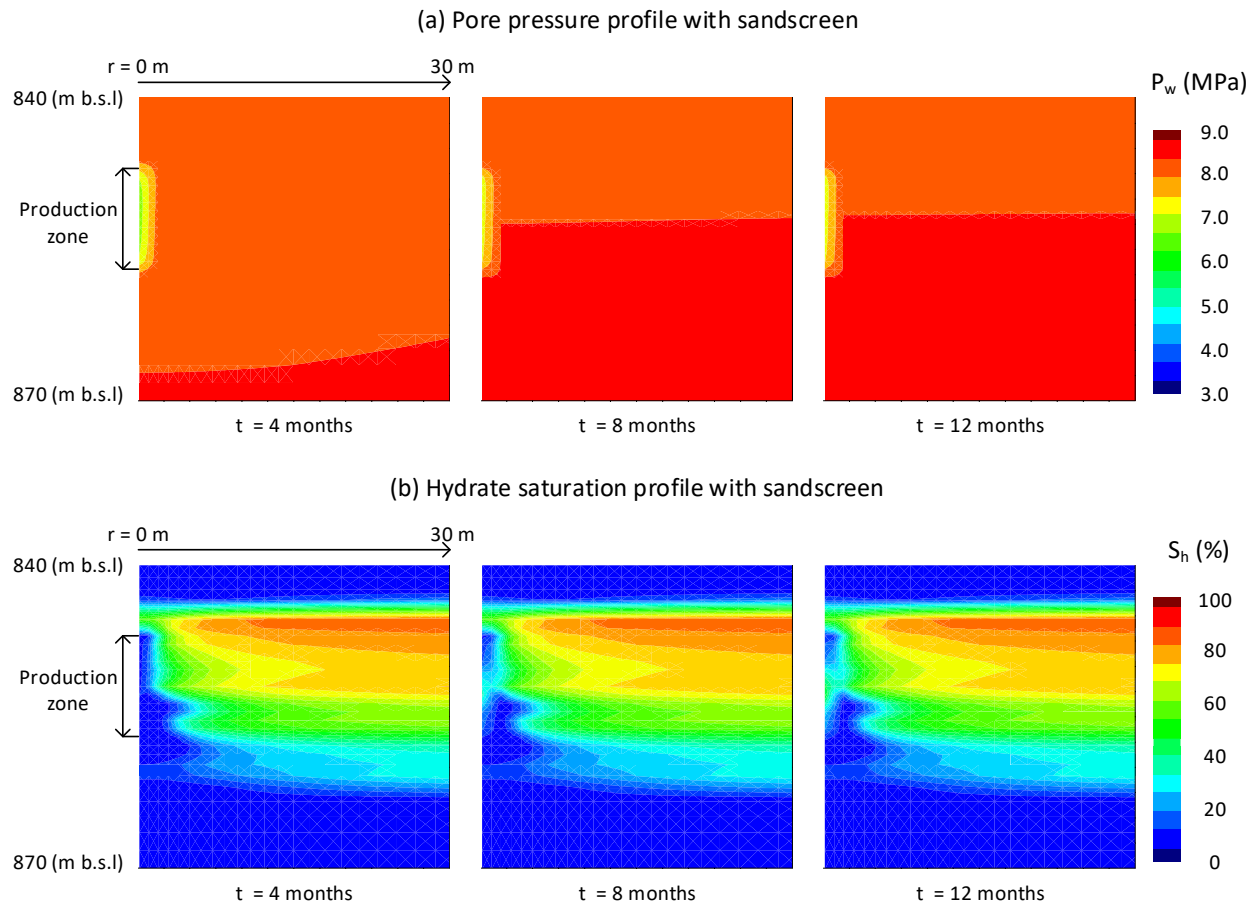


Figure 7: Reservoir responses (a) pore pressure, and (b) hydrate saturation with the sand-screen model

Fig. 9 shows the production history of gas, water and sands for the cases with and without the sandscreen model. The produced sand in the case of without the sandscreen model represents the amount of sands accumulated at the first zones. Fig. 10 shows the history of production rate of gas, water and sands. For the case without the sandscreen model, the effect of the two shut-ins on water and sand production is noticeable such that there is a significant increase in the rate just after shut-ins. This is because the pore pressure recovers around the well during the shut-in period so that the pressure gradient is very

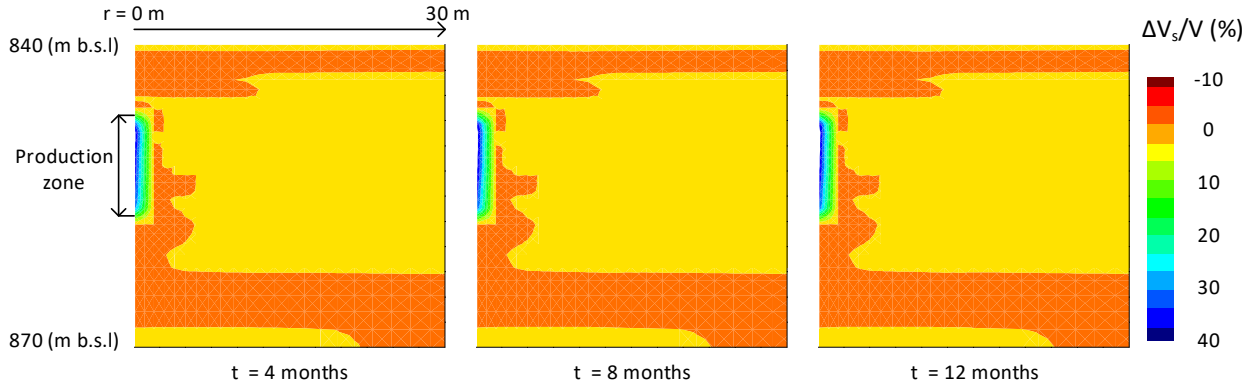


Figure 8: Change in sand volume with the sandscreen model

large at the end of shut-ins. Water and mobilized sands are available around the well, a large amount of water and sands is produced. In contrast, gas will turn into hydrates during shut-ins so there is little amount of gas left near the well at the end of shut-ins. Therefore, there is no increase in the rate of gas production. Since a large sand flow would be detrimental to well equipments, this highlights the necessity of further investigation as to whether slow re-depressurization would help to lower the rate of sand production. For the case with the sandscreen model, the production history is similar to that without screen up to approximately 2 months but almost no gas or water is produced thereafter. This is caused by the full closure (permeability reaching to zero due to accumulation of solid) assumed in this study for the sandscreen modeling. From numerical viewpoint, the amount required to block the well is proportional to the size of the element adjacent to the well and this is clearly not realistic. Consideration of limit to packing density that allows fluid flow but blocks sand migration has to be introduced for future studies.

Summary

This paper presented the sand migration evolution during gas production from gas hydrate reservoir at the Kuparuk 7-11-12 site in the Prudhoe Bay Unit, Alaska North Slope. Unlike a short-time gas hydrate production by depressurization, it is found that the sediments deform in deviatoric manner when modeled over 12 months, especially where hydrate dissociation

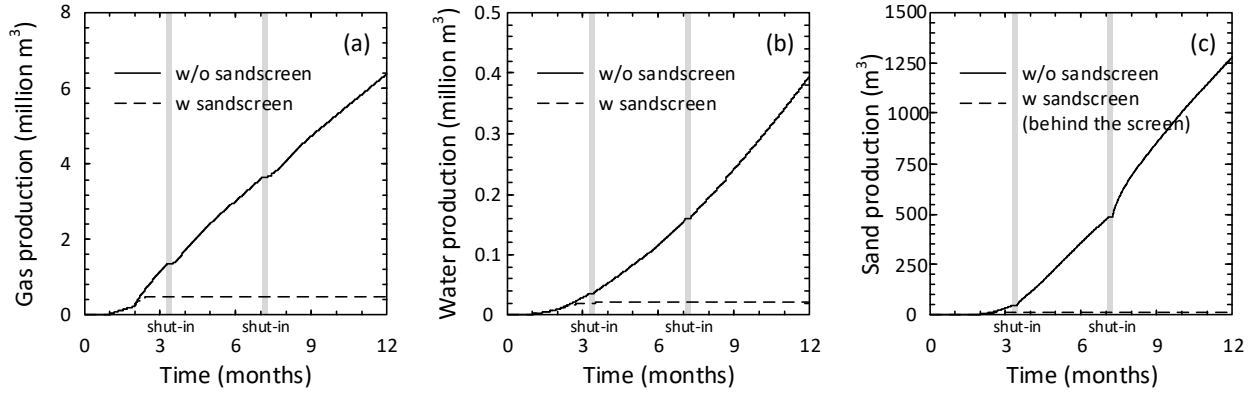


Figure 9: Production history of (a) gas, (b) water and (c) sand with and without the sandscreen model

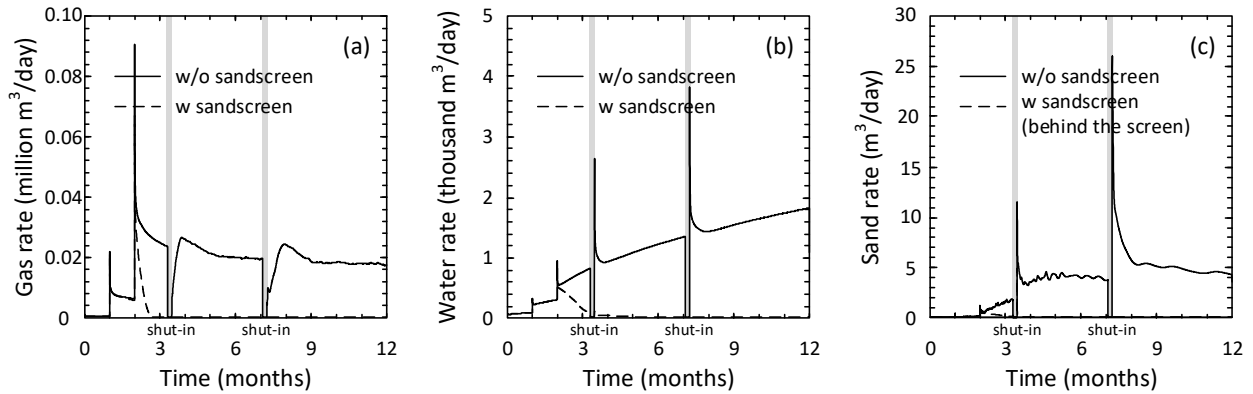


Figure 10: Production rate history of (a) gas, (b) water and (c) sand with and without the sandscreen model

occurs relatively faster. This is caused by the difference in hydrate dissociation rate at the site and also by the relatively similar stiffness yet very different strengths between hydrate-bearing and hydrate-free sediments. In addition, as an extreme event, when all the migrating sands are modeled to be entirely blocked at the well, they soon accumulate and significantly reduce the permeability. Although the amount of mobilized and migrating sands heavily relies on the parameters, this study revealed sand migration could continue throughout the one-year-long gas production and sand mobilization could extend as far away as 20-30 meters from the well at the Kuparuk 7-11-12 site.

The case of perfect sandscreen showed that the clogging of sandscreen and formation in the vicinity of the well might cause severe skin effect and inhibit gas production. The model applied here is an extreme case ignoring fines passing the screen and the limit of packing density. However, the results suggest the importance of optimization of sand control design that should consider the balance between the productivity and risk mitigation of sand production. The current design of the sand control applied to the Alaska production test consider the both merit and demerit of sand control, but other factors such as zonal isolation and resistance to erosion should be considered, too. Moreover, some mitigation plans for clogging of the sandscreen such as back-flushing and recover and exchange of devices are considered in the well design.

Acknowledgement

This study is conducted as a part of collaboration between Japan MH21-S and the NETL - U.S. Department of Energy Gas Hydrate R & D program. The authors would like to express their sincere appreciation to the Ministry of Economy, Trade and Industry of Japan (METI) and the U.S. Department of Energy for providing financial support as well as the permission to disclose this research. Neither the United States Government nor the Japanese Government, nor any agency thereof, nor any of their employees, nor the support contractor,

nor any of their employees, makes any warranty, expressed or implied, or assumes any legal liability or responsibility for the accuracy, completeness, or usefulness of any information, apparatus, product, or process disclosed, or represents that its use would not infringe privately owned rights. Reference herein to any specific commercial product, process, or service by trade name, trademark, manufacturer, or otherwise, does not necessarily constitute or imply its endorsement, recommendation, or favoring by the United States Government or the Japanese Government, or any agency thereof. The views and opinions of authors expressed herein do not necessarily state or reflect those of the United States Government or the Japanese Government, or any agency thereof.

References

- (1) Dallimore, S. R.; Wright, J. F.; Yamamoto, K.; Bellefleur, G. Proof of concept for gas hydrate production using the depressurization technique, as established by the JOGMEC/NRCan/Aurora Mallik 2007-2008 Gas Hydrate Production Research Well Program, Mackenzie Delta, Northwest Territories, Canada. *Bulletin of the Geological Survey of Canada* **2012**, *601*, 1–15.
- (2) Yamamoto, K.; Terao, Y.; Fujii, T.; Terumichi, I.; Seki, M.; Matsuzawa, M.; Kanno, T. Operational overview of the first offshore production test of methane hydrates in the Eastern Nankai Trough. Offshore Technology Conference. Houston, Texas, 2014; pp OTC-25243-MS.
- (3) Yamamoto, K.; Wang, X. X.; Tamaki, M.; Suzuki, K. The second offshore production of methane hydrate in the Nankai Trough and gas production behavior from a heterogeneous methane hydrate reservoir. *RSC Advances* **2019**, *9*, 25987–26013.
- (4) Ouchi, H.; Yamamoto, K.; Akamine, K.; Kano, S.; Naiki, M.; Tamaki, M.; Otsuki, S.; Kanno, T.; Tenma, N. Numerical history-matching of modeling and actual gas produc-

- tion behavior and causes of the discrepancy of the Nankai Trough gas-hydrate production test cases. *Energy and Fuels* **2022**, *36*, 210226.
- (5) Yamamoto, K.; Kanno, T.; Ouchi, H.; Akamine, K.; Kano, S.; Naiki, M.; Tamaki, M.; Otsuki, S.; Tenma, N. Comparison of the vertical gas-hydrate production profile with the simulation results obtained using geophysical log-based reservoir characteristics and reasons for their discrepancies in the Nankai Trough. *Energy and Fuels* **2021**, 20026–20036.
- (6) Boswell, R.; Collett, T.; Okinaka, N.; Hunter, R.; Suzuki, K.; Tamaki, M.; Yoneda, J.; Itter, D.; Haines, S.; Myshakin, E.; Moridis, G. Scientific Results of the Hydrate-01 Stratigraphic Test Well Program, Western Prudhoe Bay Unit, Alaska North Slope. *Energy and Fuels* **2022**,
- (7) Collett, T.; Zyrianova, M.; Okinaka, N.; Wakatsuki, M.; Boswell, R.; Marsteller, S.; Minge, D.; Crumley, S.; Itter, D.; Hunter, R.; Garcia-Ceballos, A.; Jin, G. Design and operations of the Hydrate-01 Stratigraphic Test Well, Prudhoe Bay Unit, Alaska North Slope. *Energy and Fuels* **2022**,
- (8) Yoneda, J.; Jin, Y.; Muraoka, M.; Oshima, M.; Suzuki, K.; Walker, M.; Otsuki, S.; Kumagai, K.; Collett, T. S.; Boswell, R.; Okinaka, N. Multiple physical properties of gas hydrate-bearing sediments recovered from Alaska North Slope 2018 Hydrate-01 Stratigraphic Test Well. *Marine and Petroleum Geology* **2021**, *123*.
- (9) Myshakin, E.; Garapati, N.; Seol, Y.; Gai, X.; Boswell, R.; Ohtsuki, S.; Kumagai, K.; Sato, M.; Suzuki, K.; Okinaka, N. Numerical simulations of depressurization-induced gas hydrate reservoir (B1 sand) response at the Prudhoe Bay Unit Kuparuk 7-11-12 pad on Alaska North Slope. *Energy and Fuels* **2022**,
- (10) Uchida, S.; Klar, A.; Yamamoto, K. Sand production model in gas hydrate-bearing

- sediments. *International Journal of Rock Mechanics and Mining Sciences* **2016**, *86*, 303–316.
- (11) Uchida, S.; Klar, A.; Yamamoto, K. Sand production modeling of the 2013 Nankai offshore gas production test. *Energy Geotechnics*. 2016; pp 451–458.
- (12) Uchida, S.; Lin, J.-S.; Myshakin, E. M.; Seol, Y.; Boswell, R. Numerical simulations of sand migration during gas production in hydrate-bearing sands interbedded with thin mud layers at site NGHP-02-16. *Marine and Petroleum Geology* **2019**, *108*, 639–647.
- (13) Uchida, S.; Seol, Y.; Yamamoto, K. Variance-based determination of dominant model parameters for sand migration in homogeneous gas hydrate-bearing reservoir. *Japanese Geotechnical Society Special Publication* **2019**, *7*, 360–365.
- (14) Tamaki, M.; Fujimoto, A.; Boswell, R.; Collett, T. Geological reservoir characterization of a gas hydrate prospect associate with the Hydrate-01 stratigraphic test well, Alaska North Slope. *Energy and Fuels* **2022**,
- (15) Masuda, Y.; Naganawa, S.; Fujita, K.; Sato, K.; Hayashi, Y. Modeling and experimental studies on dissociation of methane gas hydrates in Berea sandstone cores. *Proceedings of the 3rd International Conference on Gas Hydrate*. 1999; pp 23–31.
- (16) Kozeny, J. Uber kapillare Leitung des Wassers in Boden. *Sitzungsber. Akad. Wiss. Wien* **1927**, *136*, 271–306.
- (17) Carman, P. C. Fluid flow through granular beds. *Transactions - Institute of Chemical Engineers* **1937**, *15*, 150–166.
- (18) Uchida, S.; Soga, K.; Yamamoto, K. Critical state soil constitutive model for methane hydrate soil. *Journal of Geophysical Research* **2012**, *117*, 1–13.